ACS APPLIED MATERIALS & INTERFACES

www.acsami.org

Research Article

# Simultaneous Ultrasensitive Detection and Elimination of Drug-Resistant Bacteria by Cyclometalated Iridium(III) Complexes

Ajay Gupta,[§] Puja Prasad,[§] Shalini Gupta, and Pijus K. Sasmal*

Cite This: https://dx.doi.org/10.1021/acsami.0c11161

Read Online

ACCESS | Metrics & More | Article Recommendations | Supporting Information

**ABSTRACT:** Antimicrobial resistance has become a major threat to public health due to the rampant and empirical use of antibiotics. Rapid diagnosis of bacteria with the desired sensitivity and selectivity still, however, remains an open challenge. We report a special class of water-soluble metal-based aggregation-induced emission luminogens (AIEgens), namely, cyclometalated iridium(III) polypyridine complexes of the type $[Ir(PQ)_2(N^N)]Cl$ (**1**–**3**), where PQ = 2-phenylquinoline and N^N = 2,2′-bipyridine derivatives, that demonstrate dual capability for detection and elimination of drug-resistant bacteria in aqueous solutions. These AIEgens exhibit selective and rapid sensing of endotoxins, such as lipopolysaccharides (LPS) and lipoteichoic acid (LTA) released by the bacteria, with a detection limit in the lower nanomolar range. Targeting these naturally amplified biomarkers (approximately 1 million copies per cell) by iridium(III) complexes induces strong AIE in the presence of different Gram-negative and Gram-positive bacteria including carbapenem-resistant *A. baumannii* (CRAB) and methicillin-resistant *S. aureus* (MRSA) at concentrations as low as 1.2 CFU/mL within 5 min in spiked water samples. Detection of bacteria by the complexes is also visible to the naked eye at higher ($10^8$ CFU/mL) cell concentrations. More notably, complexes **1** and **2** show potent antibacterial activity against drug-resistant bacteria with low minimum inhibitory concentrations (MICs) $\leq 5$ $\mu$g/mL (1–4 $\mu$M) via ROS generation and cell membrane disintegrity. To the best of our knowledge, this work is the "first-in-class" example of a metal-based theranostic system that integrates selective, sensitive, rapid, naked-eye, wash-free, and real-time detection of bacteria using broad-spectrum antibiotics into a single platform. This dual capability of AIEgens makes them ideal scaffolds for monitoring bacterial contamination in aqueous samples and pharmaceutical applications.

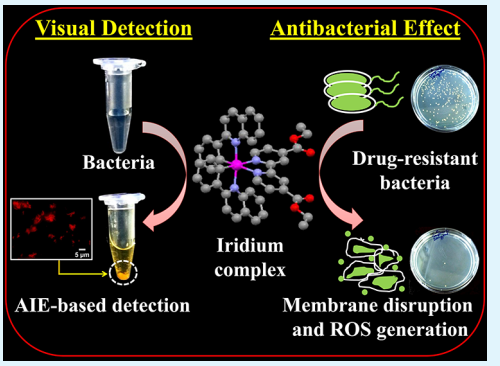


**KEYWORDS:** *cyclometalated iridium(III) complexes, aggregation-induced emission, endotoxin detection, bacterial sensing, antibacterial activity, drug-resistant bacteria, theranostic agents*



## INTRODUCTION

Discovery of the first antimicrobials 80 years ago revolutionized the traditional practice of medicine and ushered in the current era of modern surgery and treatment. Since then the rampant use of medicines and the slow innovation in new antibiotics has led to the rapid emergence of antimicrobial resistance (AMR) pushing us toward the post-antibiotics era.[1] This evolutionary phenomenon is now threatening the current paradigms of modern healthcare management and posing tangible threats to public health across the globe.[1−3] Human activity especially in developing nations has led to the contamination of water bodies with antimicrobial-resistant microbes. This water contamination as a source of AMR includes pharmaceutical industries, agriculture (in the form of pesticides), and hospital waste where a continuous efflux of antibiotics into water bodies accelerates the development and spread of resistance causing a variety of untreatable water-borne diseases.[2,4−6] Recent reports suggest how Gram-negative bacterial pathogens like *Acitenobacter baumanni* and *Klebsiella pneumonia* have developed resistance against carbapenem due to their excessive presence in river water after being discharged from general hospitals.[2,7] These data highlight the urgent and unmet need for discovering new classes of antibacterial agents and novel transformative technologies that can enable bacterial monitoring and management in water systems, including potable water, both proactively preventing and subsequently mitigating the rapid emergence of resistance.

The current classical approaches for detection of whole bacteria include cell culture,[8,9] polymerase chain reaction (PCR),[9,10] and immunoassays.[9,11] These methods, although highly popular, are also time consuming and require tedious operations with various pre-processing steps and skilled personnel.[9] On the other hand, free endotoxin, which is a

Received: June 19, 2020
Accepted: July 14, 2020
Published: July 14, 2020

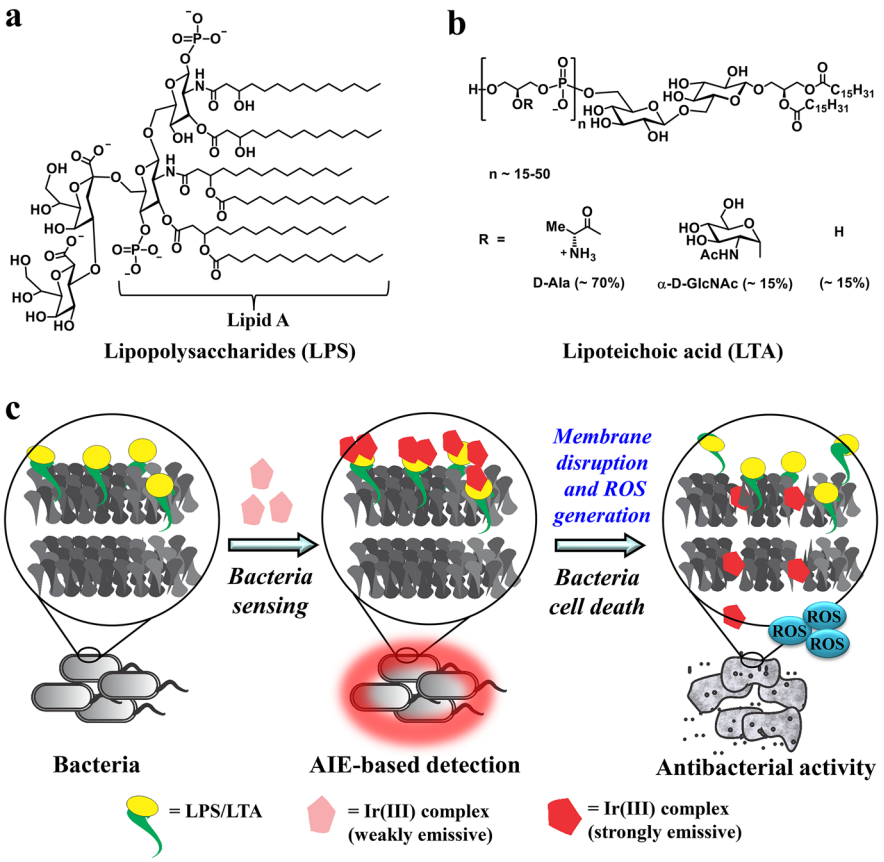


**Figure 1.** Objective of the present study. (a and b) Molecular structures of lipopolysaccharide (LPS) (a) and lipoteichoic acid (LTA) (b). (c) Proposed model for cyclometalated Ir(III) complex-mediated theranosis. Cationic Ir(III) complexes bind to the negatively charged LPS/LTA molecules either present on the bacterial surface or available freely in solution. This intermolecular association results in the facile $\pi-\pi$ stacking interactions, which leads to a strong luminescence emission and rapid bacterial sensing. Further, bacterial cell death occurs due to membrane disruption and ROS generation by the Ir(III) complexes.

major pyrogen whose contamination in drugs and pharmaceuticals is very strictly enforced by all regulatory authorities in the world, is mostly identified using the Limulus Amebocyte Lysate (LAL) test.[12,13] The LAL test, however, is exorbitantly expensive and highly dependent on key factors such as pH and temperature. An alternate test that is simple, selective, rapid, sensitive, and economical for endotoxin detection can be of immense value for screening drugs and related products in the pharmaceutical manufacturing industry. Over the past years, some advances have been made in developing new techniques such as colorimetric and electrochemical assays,[14] surface-enhanced Raman scattering (SERS),[15] mass spectrometry,[16] and peptide nucleic acid fluorescence in situ hybridization (PNA-FISH)[17] methods for bacterial detection. Recently, AIEgens turn-on probes for free endotoxin identification have emerged as promising alternatives for rapid detection of bacterial contaminants with high sensitivity.[18−25] Unlike conventional organic fluorophores, AIE fluorescent probes have unique advantages of a high quantum yield, excellent photostability, no self-quenching, and a light-up response against analytes which make them ideal scaffolds for bioimaging, sensing, and therapy applications.[26−31] In a few rare examples of AIE-derived transition metal complexes as a theranostic agent, multifunctional zinc(II)[32,33] and cyclometalated iridium(III)[34] complexes have been used as a probes for bioimaging and annihilation of bacteria.

In the present study, we sought to develop metal-based multifunctional AIE-theranostic probes for rapid, selective, ultrasensitive, and naked-eye bacterial detection and broad-spectrum antibiotics. Cyclometalated iridium(III) polypyridine complexes were found to be ideal candidates for this purpose owing to their superior photophysical properties and straightforward routes for synthesis in comparison to conventional organic fluorescent dye analogues for biomedicine, imaging, and sensing.[35−39] The luminescent nature of the Ir(III) complexes was employed for detection of bacteria mediated through the ubiquitous surface endotoxins, LPS and LTA, that are present in approximately one million copies per cell on the outer wall of all Gram-negative and Gram-positive bacteria, respectively.[40,41] To obtain the dramatic signal response with our binding probes, we leveraged the unique molecular structures of LPS and LTA. As shown in Figure 1a and 1b, LPS and LTA are highly negatively charged molecules due to the presence of multiple phosphate and/or carboxylate groups present on them. Further, these molecules contain hydrophobic regions: six alkane chains in LPS and two in LTA per structural unit. The cationic Ir(III) complexes were designed in such a way that they could cotarget two or more of these cytoskeletal regions via electrostatically mediated hydrophobic interactions to drastically improve the sensitivity of our biosensing system (Figure 1c). Targeting these naturally amplified biomarkers present on the outer wall/membrane of the bacteria using Ir(III) complexes induced a strong


https://dx.doi.org/10.1021/acsami.0c11161
ACS Appl. Mater. Interfaces XXXX, XXX, XXX−XXX

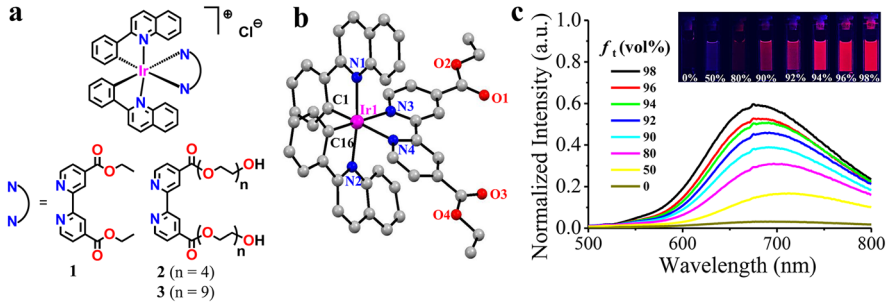


**Figure 2.** Designed iridium scaffolds and photophysical study. (a) Molecular structures of cyclometalated Ir(III) complexes (**1**−**3**) used as dual-theranostic agents in this study. (b) X-ray crystal structure of complex **1** as its $PF_6$ salt (**1a**). Hydrogen atoms and counterion have been omitted for clarity. (c) Emission spectra of complex **2** (50 $\mu$M) in a water−THF mixture with different THF fractions ($f_t$). (Inset) Corresponding phosphorescent emission images of complex **2** at room temperature in a water−THF mixture with different THF fractions ($f_t$) taken under illumination of a 365 nm UV lamp.

luminescence emission response to reach unprecedentedly low detection limits of 1.2 CFU/mL within 5 min in spiked water samples. Noteworthy, the bacteria were detectable even by the naked eye at a higher concentration. In addition, the complexes displayed potent antibacterial activity against highly drug-resistant bacteria such as CRAB and MRSA. This unique dual detection and inhibition capability of our scaffolds makes them potential contenders for a wide variety of pharmaceutical applications such as testing of parenteral drugs, biological products, etc., and monitoring and purification of environmental and potable water.

## RESULTS AND DISCUSSION

**Design and Characterization of Iridium-Based AIEgens.** The cationic bis-cylometalated iridium(III) polypyridine complexes (**1**−**3**) were synthesized to serve as bacterial theranostic agents (Figure 2a and Scheme S1). Synthesized ligands and the complexes were characterized by different analytical and spectral techniques (Figures S1−S17). The iridium(III) center was coordinated with two cyclometalating phenylquinoline (C^N) ligands and one bipyridine (N^N) that acts as an ancillary ligand to obtain a stable octahedral geometry. Complex **1** was appended with two ethyl ester moieties in the bipyridine ligand, whereas complexes **2** and **3** were appended with varying lengths of bis-polyethylene glycol (PEG) derivatives to enhance their aqueous solubility and biocompatibility and minimize cytotoxicity.[42] The Ir(III) metal ion was chosen due to its low-spin $5d^6$ outer-shell electronic configuration that is known to form kinetically inert and robust complexes.[37,43] The solid-state structure of complex **1** as its $PF_6$ salt (**1a**) was also characterized by X-ray crystallography (Tables S1 and S2 and Figure 2b). The complex crystallized in the monoclinic space group $P2_1/c$. We purified the complex as a racemic mixture and used it for further studies. No attempt was made to purify the enantiomers or to determine the enantiomeric excess.

The complexes displayed intense absorption bands in the 280−355 nm region attributed to spin-allowed intraligand ($^1$IL) $\pi \rightarrow \pi^*$ transitions for C^N and N^N ligands (Figure S18). The less intense absorption bands that appeared in the 425−430 nm region were assigned to the mixed singlet and triplet metal-to-ligand charge-transfer ($^1$MLCT and $^3$MLCT) ($d\pi$(Ir) $\rightarrow \pi^*$(N^N and C^N)) and ligand-to-ligand charge-transfer (LLCT) ($\pi$(C^N) $\rightarrow \pi^*$(N^N)) transitions.[35,39] Upon excitation at 450 nm, the complexes exhibited weak red emission bands in the range of 680−696 nm (Figure S19). The emission lifetimes of the complexes were measured to lie between 60 and 66 ns, suggesting the phosphorescent nature of these emissions,[35] and their quantum yields fell between 0.0072 and 0.0091 (Table S3 and Figure S20).

The AIE properties of cyclometalated iridium(III) complexes were investigated by varying the THF content in a water−THF mixture. Since the complexes readily solubilized in water but not in THF, the latter was used to induce aggregation of the complexes in water. The complexes were weakly emissive at ∼680 nm ($\lambda_{ex}$ = 450 nm) in aqueous solution, and the emission intensity of the complexes gradually enhanced by approximately 19-fold with shifting emission maxima (∼15 nm) as the amount of THF was increased from 0% to 98% in the mixed solutions, keeping the complex concentration same in the total solvent mixture (Figures 2c and S21). As the amount of THF increased in the mixture, aggregated particles formed.[44,45] The concurrent enhancement of the emission intensity and shifting of the emission maxima suggested unique AIE properties of the complexes.

**Aggregation-Induced Emission Detection of Bacterial Endotoxins.** As mentioned above, cyclometalated Ir(III) complexes display rich photophysical characteristics, a property that was exploited in our study for rapid detection of bacterial endotoxins. To this end, complex **2** was titrated with LPS/LTA in aqueous media at room temperature, and its phosphorescence intensity was measured after 2 min. We found that the phosphorescence intensity of this otherwise weakly emissive molecule showed a systematic LPS/LTA concentration-dependent increase in the 550−800 nm range (Figure 3a). The peaks were also slightly blue shifted. In contrast, negative control experiments performed with no LPS/LTA or LPS/LTA alone (no complex) showed a minimal change in the phosphorescence spectra (Figure S22). A plot of the emission intensity at 680 nm as a function of LPS concentration gave a linear dynamic response up to 1.4 $\mu$M (Figure 3b), and using the formula mentioned in eq S1 (see Supporting Information), the limit of detection (LOD) was found to be 4.29 nM for LPS (Table S4 and Figure 3c). This low LOD was comparable to if not better than that reported in the literature for other detection systems,[19,25,46,47] whereas complex **2** yielded an LOD value of 6.90 nM with LTA (Figure S23). When experiments were repeated with the remaining two complexes, complex **1** displayed a 2.5-fold increase in LOD with LPS and a 2-fold reduction with LTA (Figures S24 and S25), while complex **3** gave a 3−4 times higher LOD with both LPS and LTA (Table S4 and Figures S26 and S27).


https://dx.doi.org/10.1021/acsami.0c11161
ACS Appl. Mater. Interfaces XXXX, XXX, XXX−XXX

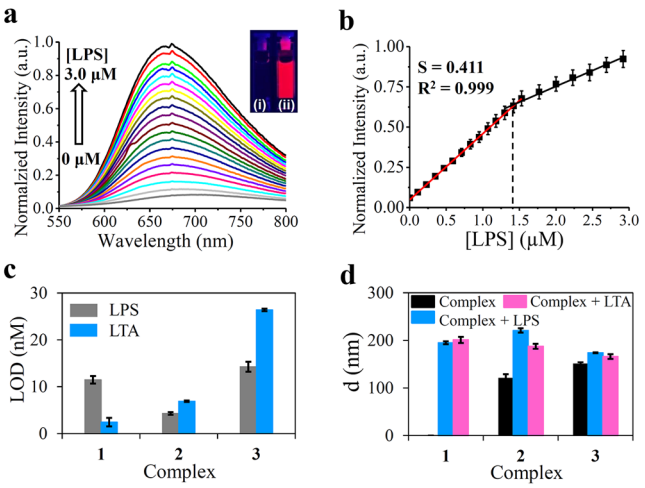


**Figure 3.** Detection of bacterial endotoxin. (a) Emission titration spectra of complex **2** (50 $\mu$M) in aqueous medium upon gradual addition of LPS (0−3 $\mu$M). (Inset) Phosphorescent emission images at room temperature of complex **2** (50 $\mu$M) under illumination of a 365 nm UV lamp in the (i) absence and (ii) presence of LPS (3 $\mu$M), respectively. (b) Plot of the emission intensity of **2** at 680 nm with LPS showing a linear dynamic range between 0 and 1.4 $\mu$M. (c) Limit of detection (LOD) of LPS and LTA by the complexes determined from the linear fit curve of emission titration using fluorescence spectroscopy. (d) Hydrodynamic diameter (d) of the complexes (50 $\mu$M) measured by dynamic light scattering (DLS) in the absence or presence of 3 $\mu$M LPS/LTA. All data are reported after 2 min of complex-LPS/LTA incubation.

We believe that this increase in emission intensity is due to the C^N and N^N ligands attached to the Ir(III) center that provide strong intermolecular $\pi-\pi$ stacking interactions of the complexes upon formation of LPS/LTA−Ir(III) aggregates.[48,49] The LPS/LTA most likely binds to the cationic Ir(III) complexes via electrostatic interactions through their negatively charged phosphate groups, and this interaction is further facilitated by hydrophobic interactions through the alkyl chains on the LPS/LTA molecules. This dual mode of interaction was found to be unique to these molecules as various other biologically relevant molecules such as the negatively charged lipid A, phosphate, adenosine triphosphate (ATP), calf-thymus DNA (ct-DNA), ethylenediaminetetraacetic acid (EDTA), sodium dodecyl sulfate (SDS), bovine serum albumin (BSA), L-glutamate (Glu), acetate, nitrate, and sulfide, positively charged phosphatidylcholine (PC), $NAD^+$, L-histidine (His), $CuSO_4$, and $ZnCl_2$, and neutral molecules like glucose, guanine, and L-cysteine (Cys) failed to show any significant change in signal (Figure S28). A marginally higher emission intensity seen in the case of lipid A, SDS, and ct-DNA (relative to other controls) corroborated with our hypothesis of electrostatically mediated hydrophobic interaction. Thus, in conclusion, complex **2** was found to be highly selective for LPS/LTA detection. The reduced tendency of complex **3** to interact with LPS/LTA was attributed to its higher extent of self-aggregation.

The results of our emission titration studies were further confirmed by a number of orthogonal techniques like dynamic light scattering (DLS), zeta potential ($\xi$) measurements, and transmission electron microscopy (TEM). DLS was carried out to determine the hydrodynamic size distributions of the Ir(III) complexes in the absence and presence of endotoxins. The hydrodynamic size of complex **1** was undetectable in the absence of LPS/LTA, whereas complexes **2** and **3** bearing PEG chains on the N^N ligands showed reasonably high hydrodynamic diameters (>120 nm) even in the absence of LPS/LTA (Table S4 and Figures 3d and S29−S31). These high hydrodynamic diameters of complexes **2** and **3** were suspected to be due to the self-aggregation of these molecules, as the presence of long hydrophilic PEG chains and hydrophobic aromatic ligand moieties (C^N and N^N) tend to promote micellization. This was also confirmed by TEM study (Figure S32a). Addition of LPS/LTA was accompanied by a significant increase in the hydrodynamic sizes in all the cases, which confirmed the successful interaction between Ir(III) complex and LPS/LTA. Direct evidence of binding in complex **2** was given by TEM, which demonstrated that the complex was considerably more aggregated in the presence of LPS/LTA (Figure S32b and S32c). Similarly, zeta potential measurements showed that the average negative charge on LPS molecules ($\xi$ = −32.7 ± 2.95 mV due to the presence of abundant phosphate groups) dropped systematically as a function of complex **1**−**3** concentration as they were put in 3−17 molar excess in the aqueous solution, indicating an electrostatic mode of binding (Table S5). Analogous experiments with LTA could only be reproduced by reverse addition wherein the $\xi$ potential of the complexes was measured upon addition of varying amounts of LTA. Once again, the average positive charge on complexes **1**−**3** (+34.5 mV < $\xi$ < +44.5 mV) gradually decreased upon addition of increasing concentrations of LTA, implying electrostatically mediated interaction between Ir(III) complex and LPS/LTA (Table S6). To further investigate the practical applicability of Ir(III) complexes for endotoxin detection in real conditions, we examined the effect of pH on complexes **1** and **2** in the presence of LPS or LTA. The results showed that the phosphorescence intensity at 680 nm indeed did not change significantly for only complex or complex in the presence of LPS or LTA in a wide pH range from 4 to 9 (Figure S33), making our complexes more superior to their existing analogues.

**Antibacterial Activity of Iridium Complexes.** The results for the interaction of complexes **1**−**3** with LPS/LTA encouraged us to investigate their potential for antimicrobial activity in a variety of Gram-negative and Gram-positive bacteria including the resistant strains. Recently, Sadler et al. also demonstrated that organometallic Ir(III) complexes containing chelating biguanide ligand exhibit potent activity against Gram-negative and Gram-positive bacteria.[43] Several studies have proven that the balance of lipophilicity and hydrophilicity plays a vital role in the cellular uptake of drugs.[50] Therefore, before initiating the antibacterial studies, we first checked the lipophilicity index (log $P_{o/w}$ value) of our complexes by measuring their partition coefficient in an *n*-octanol/water system using the classical flask-shaking method.[51] The results summarized in Table S7 showed that the lipophilicity index of complexes **1**, **2**, and **3** decreased as 1.89, −0.78 and −1.01, respectively, with increasing hydrophilic character, which indicated that the complexes were moderately lipophilic. Thus, these molecules were taken forward for antimicrobial testing.

**MIC Determination.** Next, the minimum inhibitory concentrations (MICs) of our complexes were determined against the ESKAPE group of bacteria (World Health Organization's top priority list of pathogens). These were, namely, the Gram-positive bacteria *Enterococcus faecium* (*E.*


https://dx.doi.org/10.1021/acsami.0c11161
ACS Appl. Mater. Interfaces XXXX, XXX, XXX−XXX

*faecium*) and methicillin-sensitive *Staphylococcus aureus* (*S. aureus*) (MSSA) and Gram-negative bacteria carbapenem-sensitive *Acinetobacter baumannii* (*A. baumannii*) (CSAB). In addition, *Escherichia coli* (*E. coli*), *Salmonella typhi* (*S. typhi*), carbapenem-resistant *A. baumannii* (CRAB), and methicillin-resistant *S. aureus* (MRSA) were also tested. Our results showed that complexes **1** and **2** were highly potent against all types of bacteria, except *S. typhi*, with MIC values ≤ 5 μg/mL (1−4 μM) in all cases (Table S8 and Figures 4a, S34, and S35). Exceptionally good efficacy was found against CRAB and MRSA when compared to existing antibiotics vancomycin and polymyxin B sulphate. In all the other cases too, complexes **1** and **2** showed comparable performance to vancomycin. On the other hand, polymyxin B was found to be active only against *S. typhi* (MIC < 1 μg/mL (or < 0.76 μM) and showed ≥30 μg/mL (or ≥23.04 μM) MIC against all other bacteria. Overall, complex **1** was found to be slightly more superior than **2** for all of the pathogens and interestingly showed more activity against the resistant bacteria as compared to their wild types. Complex **3**, however, showed only moderate activity against MRSA, MSSA, CRAB, and CSAB (MIC in the range of 20−30 μg/mL (12.16−18.24 μM)) and was found to be ineffective against *E. coli*, *E. faecium*, and *S. typhi* (MIC > 30 μg/mL or >18.24 μM). This observation correlated with our detection results (Table S4) and is again thought to be a result of the reduced interaction between complex **3** and the bacterial surface. This also corroborates well with the lipophilicity (log $P_{o/w}$) experimental results that suggest that the uptake of compounds within bacterial membranes increases with lipophilic character. Therefore, it was suspected that complex **1** would be most active against both Gram-negative and Gram-positive bacteria due to its lipophilic nature. However, none of the ligands (**L1**−**L3**) alone showed antibacterial activity against any of the bacteria and exhibited MIC > 30 μg/mL (or > 28.88 − > 99.61 μM) (Table S8 and Figures S36 and S37).

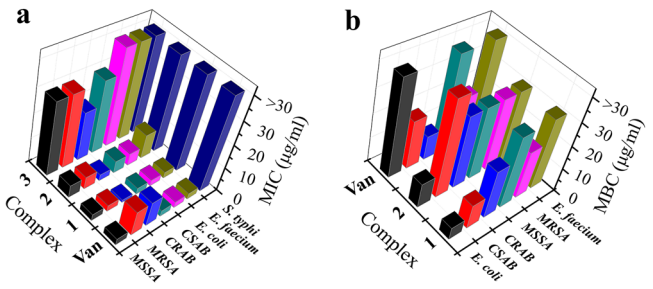


**Figure 4.** Antibacterial activity studies. (a) MIC values of complexes **1**−**3** and vancomycin (Van). (b) MBC values of complexes (**1** and **2**) and Van obtained against different bacterial strains. Error bars are omitted for clarity. See Tables S8 and S9 for specific values.

To further determine the minimum bactericidal concentrations (MBCs) of complexes **1** and **2**, we examined their antibacterial activity in both Gram-negative and Gram-positive bacteria and compared the results to vancomycin (Table S9 and Figures 4b and S38−S40). The MBC value was determined by taking aliquots from the wells showing less or no turbidity in the MIC experiments and replating them on agar plates. The concentration where no bacterial colony was observed was termed the MBC. The MBC/MIC ratio that decides whether the death caused by the compound is bacteriostatic or bactericidal in nature was found to be ≤4 for complex **1** against CSAB and *E. coli* and for complex **2** against *E. coli* and *E. faecium*, indicating that cell death was bactericidal in these cases. On the other hand, MBC/MIC was found to be >4 for complexes **1** and **2** against all other bacteria, suggesting a bacteriostatic mode of cell death. Vancomycin showed bacteriostatic cell death in all the cases except CRAB and MRSA.

**Mechanism of Drug Action.** The most likely mechanisms for bacterial cell damage by complexes **1** and **2** were hypothesized to be cell membrane disintegration and generation of reactive oxygen species (ROS). To quantify the amount of ROS generated in our system, a time-dependent dichlorofluorescein diacetate (DCFH-DA) assay was carried out in which a cell-permeable fluorogenic probe DCFH-DA that undergoes oxidation to form 2′,7′-dichlorofluorescein (DCF) with a maximum emission at 528 nm and fluorescence intensity proportional to ROS concentration. Thus, different concentrations of complex **1** or **2** were incubated with MSSA, MRSA, CSAB, or CRAB. The results showed that the fluorescence intensity was enhanced over time in a dose-dependent manner, confirming ROS generation (Figures 5a, 5b, and S41−S43). Also, the fluorescence intensity at all times was higher in complex **1** than in complex **2**, suggesting that the former had greater antibacterial potency. This was in agreement with our results in Figure 4.

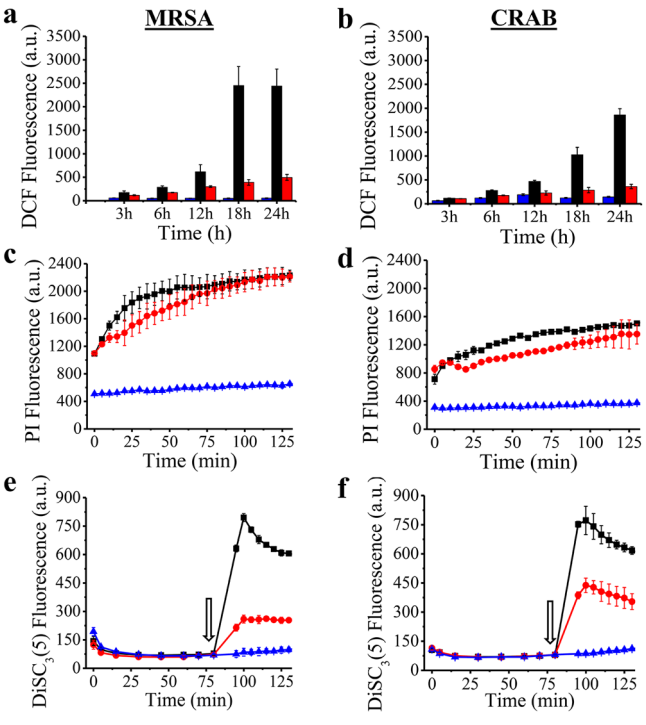


**Figure 5.** Mechanistic aspects of antibacterial activity. (a and b) Quantification of ROS generation by DCFDA dye at different time intervals after treatment with 5 μg/mL (or 5.33 μM) complex **1** and 5 μg/mL (or 4.01 μM) complex **2**. (c−f) Time-resolved fluorescence spectroscopy data obtained for membrane permeabilization (c and d) and membrane depolarization (e and f) events using PI and $DiSC_3(5)$ dyes, respectively. Figures a, c, and e and b, d, and f were studied in MRSA and CRAB, respectively. Blue, black, and red bars and symbols imply control (no complex), complex **1** (5 μg/mL), and complex **2** (5 μg/mL), respectively. Arrows in graphs e and f represent the addition of complex at that point.


https://dx.doi.org/10.1021/acsami.0c11161
ACS Appl. Mater. Interfaces XXXX, XXX, XXX−XXX

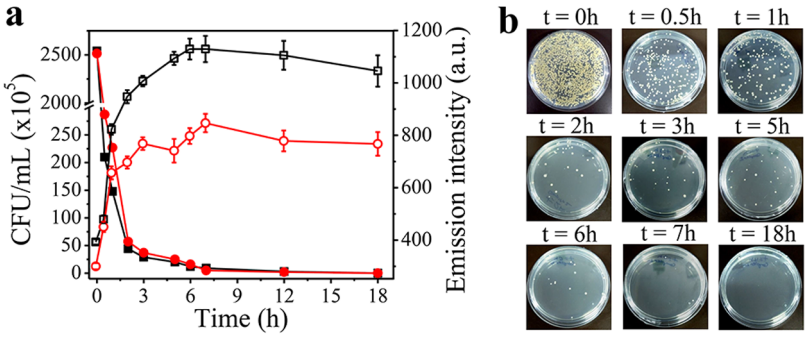


**Figure 6.** Theranostic capability of iridium probes. (a) Kinetics of bacterial detection using fluorescence spectroscopy (hollow data points) and growth inhibition by the counting method using agar plates (solid data points) in carbapenem-resistant *A. baumannii* (CRAB) by 15 $\mu$g/mL (or 16.01 $\mu$M) complex **1** (□, ■) and 15 $\mu$g/mL (or 12.05 $\mu$M) complex **2** (○, ●) in aqueous medium. (b) Kinetics of growth inhibition of CRAB treated with 15 $\mu$g/mL complex **2** in aqueous medium. Bacterial inhibition was monitored using agar plates.

Similarly, the membrane-targeting mechanism of action was investigated in all four bacteria by assessing the changes in their cytoplasmic membrane permeabilization and membrane potential using fluorescence spectroscopy. For membrane permeabilization experiments, propidium iodide (PI) dye was used as it selectively enters the cytosol of bacteria whose membrane has been compromised and fluoresces at 617 nm upon binding to the DNA. Thus, any real-time change in bacterial membrane permeability can be picked up easily by measuring the fluorescence response. Our results showed that the PI fluorescence intensity was significantly more enhanced in complexes **1** and **2** as compared to the control (no complex) case, indicating that both complexes were able to effectively permeabilize the cytoplasmic membrane of the bacteria irrespective of their gram status (Figure 5c, 5d, and S43). Marginally higher fluorescence intensities were detected in complex **1** than in complex **2**, as expected from our above results. For the cytoplasmic membrane depolarization studies, a voltage-sensitive fluorescent dye called 3,3′-dipropylthiadicarbocyanine iodide ($DiSC_3 5$) was used. This cationic dye fluoresces at 670 nm and is capable of penetrating lipid bilayers and accumulating inside polarized bacterial cells, leading to its fluorescence quenching. The fluorescence intensity can be recovered once the dye diffuses back into the media upon bacterial membrane disintegration due to stress-induced depolarization. When cells were treated with this dye our results too showed initial quenching but upon addition of complexes **1** and **2** displayed a rapid increase in fluorescence intensity compared to controls, confirming that complexes **1** and **2** were both membrane active (Figures 5e, 5f, and S43). On the basis of the level of fluorescence enhancement, complex **1** appeared to be a faster-acting drug compared to **2** in agreement with all our experimental results presented so far.

Several mechanistic studies in the literature reveal that a two-step mechanism could be involved in the interaction between the bacteria and the Ir(III) complexes.[52] This involves increased ROS production of mainly hydroxyl radicals and singlet oxygen and the accumulation of Ir(III) complexes on the surface of bacteria, causing disruption and disorganization of the cell membrane. In our case, the membrane permeabilization and depolarization effects were observed within 1−2 h upon treatment with the complexes, whereas ROS generation showed an exponential increase after 12 h, indicating ROS generation was involved as a secondary pathway in the killing of bacteria. Therefore, from the above results, we believe that the Ir(III) complexes first bind electrostatically with the LPS/LTA present on the outer membrane of bacteria, resulting in some sort of dislodging and loss of membrane integrity. Finally, the complexes enter inside the bacterial cytoplasm, leading to ROS-mediated cell death. This dual mode of bacterial annihilation is highly beneficial compared to conventional antibiotics in which a gain in resistance is easier due to specific targets. ROS, on the other hand, provides random oxidation of DNA, RNA, protein, and/or lipid, leading to bacterial destruction and thus prevents development of any specific resistance mechanisms in bacteria.[32,53]

**Dual Functionality of Iridium Complexes for Rapid Detection and Targeting of Whole Bacteria.** So far, we have successfully illustrated how our iridium complexes can be separately used for detecting free bacterial endotoxins (LPS and LTA) and for killing of both Gram-negative and Gram-positive classes of bacteria in an equally efficient manner. Since bacteria actively shed endotoxins during their life cycle or as they undergo external stress-induced cell death, we further hypothesized that our unique iridium scaffolds could even be applied for rapid detection of whole bacteria, allowing simultaneous cell removal and death monitoring in a single setup without using any external molecular detection probes. This could be a major step forward in the way live bacterial contaminants, posing a major health hazard, are assessed in potable water, food products, and biopharmaceutical formulations. To test our hypothesis, endotoxin-free water was spiked with CRAB along with complex **1** or **2**, and its emission response and viable cell concentration was measured as a function of time. Indeed, the kinetic plots of emission intensity showed an upward monotonic trend until the signal reached saturation around 7 h once all of the bacteria in the system (starting concentration $2.5 \times 10^8$ CFU/mL) were dead (Figures 6 and S44). The earliest response could be measured as early as 30 min into the assay using both complexes. These results clearly established the theranostic capabilities of our molecules and the great promise they hold for dual monitoring and treatment of bacteria-infected samples.

Another advantage of our system was the simplicity and the broad tunability of the assay in terms of the time and concentration range required for cell detection. Using $10^8$ CFU/mL cells and 400 $\mu$g/mL (or 420 $\mu$M) of complex **1** or 400 $\mu$g/mL (or 320 $\mu$M) of complex **2**, we found that the bacteria agglutinated immediately and formed large pellets at the bottom of the eppendorf tubes which could be visualized by the naked eye within just 10 min (Figure 7a). The naked-


https://dx.doi.org/10.1021/acsami.0c11161
ACS Appl. Mater. Interfaces XXXX, XXX, XXX−XXX

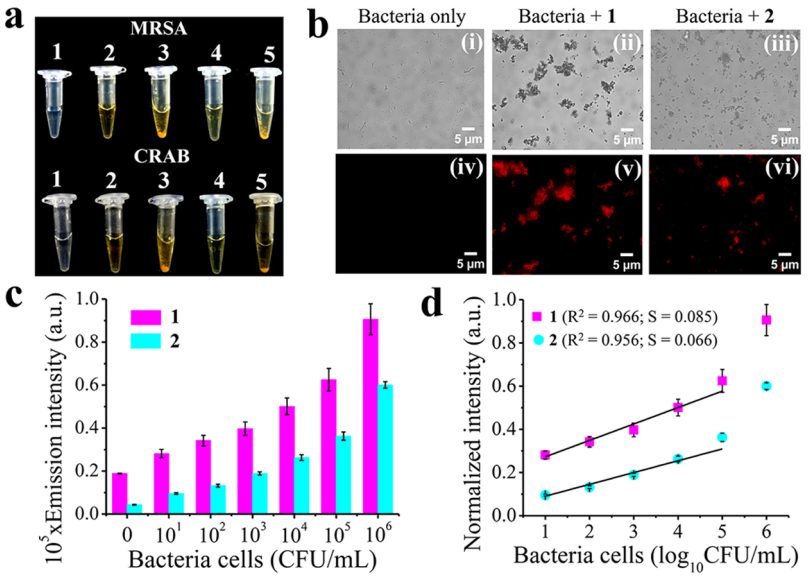


**Figure 7.** Bacteria sensing studies. Rapid bacterial agglutination test in spiked water samples visualized by (a) the naked eye, (b) optical microscopy, and (c, d) fluorescence spectroscopy. In a, $10^8$ CFU/mL MRSA and CRAB were treated with 400 $\mu$g/mL (or 420 $\mu$M) complex **1** and 400 $\mu$g/mL (or 320 $\mu$M) complex **2**. Labels: 1, only bacteria; 2, only complex **1**; 3, complex **1** + bacteria; 4, only complex **2**; 5, complex **2** + bacteria. In b,$10^8$ CFU/mL of MRSA was treated with 400 $\mu$g/mL complex **1** and **2**, and results were observed in complementary bright-field (i–iii) and fluorescence (iv–vi) modes. Here, left panels indicate results for bacteria only, middle panels for bacteria treated with complex **1**, and right panels for bacteria treated with complex **2**. In c, different concentrations ($10^1$–$10^6$ CFU/mL) of CRAB were treated with 50 $\mu$g/mL (or 53 $\mu$M) complex **1** and 50 $\mu$g/mL (or 40.1 $\mu$M) complex **2**, and its phosphorescence emission intensity was measured after 5 min. In d, the LODs of CRAB by complexes **1** and **2** were determined from the linear fit calibration curve using fluorescence spectroscopy in the range from $10^1$ to $10^5$ CFU/mL.

eye detection of bacteria-spiked water samples is one of the first such examples using metal complexes. Fluorescence optical micrographs of these samples displayed a strong red emission, confirming Ir(III)-complex-mediated cell aggregation (Figures 7b(ii, iii, v, and vi) and S45), whereas control samples with only bacteria appeared blank (Figure 7b(i, iv). Adjusting the relative concentration of the complexes and cells could also control the agglutination kinetics. For instance, lowering the complex concentration by one-half (to 200 $\mu$g/mL) doubled the naked-eye visualization time to 20 min for $10^8$ CFU/mL bacteria. Furthermore, fluorescence spectroscopy data showed concentration-dependent detection of bacteria in the range of $10^1$–$10^6$ CFU/mL within only 5 min (Figure 7c). The linear dynamic range of the assay extended over 5 orders of magnitude ($10^1$–$10^5$ CFU/mL) for complexes **1** and **2** and gave LODs of 1.2 ± 0.5 and 1.5 ± 0.3 CFU/mL, respectively, using eq S1 (Figure 7d). This low-concentration detection was made possible due to the approximately million-fold increase in the LPS/LTA biomarker concentration (per cell) that could be picked up rather easily by our system. To the best of our knowledge, this low limit of detection is one of the best reported to date with small molecules. Thus, we provide a sensitive yet simple, wash-free, low-cost, and real-time method to monitor bacterial contamination in aqueous samples.

**Cytotoxicity Studies.** Finally, to establish the full potential of our molecules for any real-life application, the cytotoxicity of complexes **1**–**3** was investigated against model human red blood cells (RBCs) and human embryonic kidney cells (HEK 293) to know the specificity of our molecules toward bacteria. For this, the hemolytic activity of the complexes was reported in terms of $HC_{50}$ values or the concentration of complexes at which 50% of the RBCs got lysed. The $HC_{50}$ values in all the cases were found to be reasonably high (>25 $\mu$g/mL or 27.76–37.76 $\mu$M), which corresponded to 10× MIC values of the respective complexes. More notably, the hemolytic activity was seen to vary inversely proportional to the PEG chain length (Table S7 and Figure S46). Similarly, the cytotoxicity ($IC_{50}$) of the complexes in HEK 293 cells was found to be 3–4 times the MIC value determined using MTT assays (Table S7 and Figure S47). These results showed moderate biocompatibility of our complexes with mammalian cells. On the basis of the literature, these results are not unexpected and imply that the incorporation of a hydrophilic moiety in the positively charged iridium headgroup may be necessary as a trade-off to balance the complex's antimicrobial and cytotoxic activity.[S4] In other words, complex **2** bearing the $PEG_{200}$ chain may after all be the best candidate to take forward as an antimicrobial drug for in vivo purposes.

## CONCLUSIONS

In summary, we have developed a simple and robust system for rapid and simultaneous detection and inhibition of drug-resistant bacteria using novel cyclometalated iridium(III) complexes (**1**–**3**). Complexes **1** and **2** were found to be more superior as antibacterial and biosensing agents. These complexes showed AIE-based detection of endotoxin (LPS and LTA) in a lower nanomolar range in aqueous media. More notably, both complexes were highly selective toward LPS/LTA detection compared to common biomolecules. In the case of whole bacterial cell detection, concentrations as low as 1.2 CFU/mL were reliably detected spectroscopically within 5 min in aqueous solution, and is one of the best reported to date by small molecules. Also, at higher concentrations of $10^8$ CFU/mL, rapid bacterial agglutination could be detected by the naked eye in only 10 min, which is also the first such example by metal complexes. This can be particularly useful for quick yes/no-type screening of water samples containing high loads of bacterial contamination in resource-poor settings.


https://dx.doi.org/10.1021/acsami.0c11161
ACS Appl. Mater. Interfaces XXXX, XXX, XXX–XXX

Both complexes **1** and **2** also exhibited potent antibacterial activity with low MIC values (≤5 μg/mL or 1−4 μM) comparable to existing antibiotics against a wide range of high-priority Gram-negative and Gram-positive bacteria, including MRSA and CRAB. The cytotoxicity studies suggested higher specificity of our compounds toward bacterial cells compared to mammalian cells, and the specificity increased upon introduction of a PEG moiety. The mechanism of cell death was found to be loss of membrane integrity followed by ROS generation. Overall, the simple affordable design strategy and dual theranostic capability of our system lends itself to further investigation for commercial exploitation as the chemical syntheses procedures can be easily scaled to meet the demands of routine quality testing of many pharmaceutical formulations before they are accepted and released as finished products. In addition, detection of coliform contamination in potable water could save many lives and lower the total consumption of antibiotics in our society, in turn curbing the problem of AMR.

## ■ ASSOCIATED CONTENT

### Supporting Information

The Supporting Information is available free of charge at https://pubs.acs.org/doi/10.1021/acsami.0c11161.

Experimental details, synthetic procedures, characterization data, crystallographic data, biological studies (endotoxin and bacteria sensing studies and antibacterial activity), figures, and tables (PDF)

Crystallographic data of CCDC 1969746 (CIF)

## ■ AUTHOR INFORMATION


### Corresponding Author

**Pijus K. Sasmal** − *School of Physical Sciences, Jawaharlal Nehru University, New Delhi 110067, India;* orcid.org/0000-0002-2301-1269; Email: pijus@mail.jnu.ac.in

### Authors

**Ajay Gupta** − *School of Physical Sciences, Jawaharlal Nehru University, New Delhi 110067, India*

**Puja Prasad** − *Department of Chemical Engineering, Indian Institute of Technology Delhi, New Delhi 110016, India*

**Shalini Gupta** − *Department of Chemical Engineering, Indian Institute of Technology Delhi, New Delhi 110016, India;* orcid.org/0000-0003-1382-0254

Complete contact information is available at: https://pubs.acs.org/10.1021/acsami.0c11161

### Author Contributions

[§]A.G. and P.P. contributed equally to this work.


### Author Contributions

P.K.S. and P.P. conceived the project idea. A.G. carried out the synthesis and characterization of the compounds. A.G. performed sensing interaction studies of the compounds with LPS and LTA. P.P. performed all of the biological studies such as imaging of bacteria and antibacterial activity. All authors were involved in the design and interpretation of the experiments. The manuscript was written with contributions of all authors. All authors have given approval to the final version of the manuscript.

### Notes

The authors declare no competing financial interest.

## ■ ACKNOWLEDGMENTS

P.K.S. acknowledges SERB, DST (ECR/2016/000810), UPE-II (Project No. 256), and DST-PURSE for financial support. S.G. acknowledges DST Nanomission (SR/NM/NT-1049/2016). We thank DST for the Single Crystal XRD facility in SPS, JNU, and AIRF, JNU for the instrumentation facilities. P.P. thanks CSIR for the SRA position (Pool No. 9031-A) and SERB-DST for funding (NPDF/2016/000087). A.G. thanks UGC for a fellowship. Dr. S. Sen, SPS, JNU, is gratefully acknowledged for generously allowing us to use the spectrofluorometer. We sincerely thank Dr. D. Das and A. Shrivastava, SPS, JNU, for help with X-ray data collection and solving the crystal structure of **1a**. We thank Dr. B. K. Sarma, JNCASR, for helpful discussions.

## ■ REFERENCES


(1) *Antimicrobial Resistance: Global Report on Surveillance*; World Health Organization: Geneva, Switzerland, 2014; http://www.who.int/drugresistance/documents/surveillancereport/en/ (accessed Sept 3, 2015).

(2) Ferri, M.; Ranucci, E.; Romagnoli, P.; Giaccone, V. Antimicrobial Resistance: A Global Emerging Threat to Public Health Systems. *Crit. Rev. Food Sci. Nutr.* **2017**, *57*, 2857−2876.

(3) Fair, R. J.; Tor, Y. Antibiotics and Bacterial Resistance in the 21st Century. *Perspect. Med. Chem.* **2014**, *6*, 25−64.

(4) Prestinaci, F.; Pezzotti, P.; Pantosti, A. Antimicrobial Resistance: A Global Multifaceted Phenomenon. *Pathog. Global Health* **2015**, *109*, 309−318.

(5) Ramirez-Castillo, F. Y.; Loera-Muro, A.; Jacques, M.; Garneau, P.; Avelar-González, F. J.; Harel, J.; Guerrero-Barrera, A. L. Waterborne Pathogens: Detection Methods and Challenges. *Pathogens* **2015**, *4*, 307−334.

(6) Bengtsson-Palme, J.; Kristiansson, E.; Larsson, D. G. J. Environmental Factors Influencing the Development and Spread of Antibiotic Resistance. *FEMS Microbiol. Rev.* **2018**, *42*, 68−80.

(7) Hrenovic, J.; Durn, G.; Kazazic, S.; Dekic, S.; Music, M. S. Untreated Wastewater as Source of Carbapenam-Resistant Bacteria to the Riverine Ecosystem. *Water SA* **2019**, *45*, 55−62.

(8) Fratamico, P. M. Comparison of Culture, Polymerase Chain Reaction (PCR), TaqMan *Salmonella*, and Transia Card *Salmonella* Assays for Detection of *Salmonella* spp. in Naturally-Contaminated Ground Chicken, Ground Turkey, and Ground Beef. *Mol. Cell. Probes* **2003**, *17*, 215−221.

(9) Rajapaksha, P.; Elbourne, A.; Gangadoo, S.; Brown, R.; Cozzolino, D.; Chapman, J. A Review of Methods for the Detection of Pathogenic Microorganisms. *Analyst* **2019**, *144*, 396−411.

(10) Rodriguez-Lazaro, D.; Hernandez, M.; Esteve, T.; Hoorfar, J.; Pla, M. A Rapid and Direct Real Time PCR-Based Method for Identification of *Salmonella* spp. *J. Microbiol. Methods* **2003**, *54*, 381−390.

(11) Wolff, L. F.; Anderson, L.; Sandberg, G. P.; Aeppli, D. M.; Shelburne, C. E. Fluorescence Immunoassay for Detecting Periodontal Bacterial Pathogens in Plaque. *J. Clin. Microbiol.* **1991**, *29*, 1645−1651.

(12) Roslansky, P. F.; Novitsky, T. J. Sensitivity of *Limulus* Amebocyte Lysate (LAL) to LAL-Reactive Glucans. *J. Clin. Microbiol.* **1991**, *29*, 2477−2483.

(13) Zhang, G.-H.; Baek, L.; Nielsen, P. E.; Buchardt, O.; Koch, C. Sensitive Quantitation of Endotoxin by Enzyme-Linked Immunosorbent Assay with Monoclonal Antibody Against *Limulus* peptide C. *J. Clin. Microbiol.* **1994**, *32*, 416−422.

(14) Sun, J.; Warden, A. R.; Huang, J.; Wang, W.; Ding, X. Colorimetric and Electrochemical Detection of *Escherichia coli* and Antibiotic Resistance Based on a *p*-Benzoquinone-Mediated Bioassay. *Anal. Chem.* **2019**, *91*, 7524−7530.

(15) Gao, W.; Li, B.; Yao, R.; Li, Z.; Wang, X.; Dong, X.; Qu, H.; Li, Q.; Li, N.; Chi, H.; Zhou, B.; Xia, Z. Intuitive Label-Free SERS

Detection of Bacteria Using Aptamer-Based in Situ Silver Nanoparticles Synthesis. *Anal. Chem.* **2017**, *89*, 9836−9842.
(16) Zhu, Y.; Gasilova, N.; Jović, M.; Qiao, L.; Liu, B.; Lovey, L. T.; Pick, H.; Girault, H. H. Detection of Antimicrobial Resistance-Associated Proteins by Titanium Dioxide-Facilitated Intact Bacteria Mass Spectrometry. *Chem. Sci.* **2018**, *9*, 2212−2221.
(17) Mach, K. E.; Kaushik, A. M.; Hsieh, K.; Wong, P. K.; Wang, T. H.; Liao, J. C. Optimizing Peptide Nucleic Acid Probes for Hybridization-Based Detection and Identification of Bacterial Pathogens. *Analyst* **2019**, *144*, 1565−1574.
(18) Kang, M.; Zhou, C.; Wu, S.; Yu, B.; Zhang, Z.; Song, N.; Lee, M. M. S.; Xu, W.; Xu, F.-J.; Wang, D.; Wang, L.; Tang, B. Z. Evaluation of Structure-Function Relationships of Aggregation-Induced Emission Luminogens for Simultaneous Dual Applications of Specific Discrimination and Efficient Photodynamic Killing of Gram-Positive Bacteria. *J. Am. Chem. Soc.* **2019**, *141*, 16781−16789.
(19) Jiang, G.; Wang, J.; Yang, Y.; Zhang, G.; Liu, Y.; Lin, H.; Zhang, G.; Li, Y.; Fan, X. Fluorescent Turn-on Sensing of Bacterial Lipopolysaccharide in Artificial Urine Sample with Sensitivity Down to Nanomolar by Tetraphenylethylene Based Aggregation Induced Emission Molecule. *Biosens. Bioelectron.* **2016**, *85*, 62−67.
(20) He, X.; Xiong, L.-H.; Zhao, Z.; Wang, Z.; Luo, L.; Lam, J. W. Y.; Kwok, R. T. K.; Tang, B. Z. AIE-Based Theranostic Systems for Detection and Killing of Pathogens. *Theranostics* **2019**, *9*, 3223−3248.
(21) Feng, G.; Yuan, Y.; Fang, H.; Zhang, R.; Xing, B.; Zhang, G.; Zhang, D.; Liu, B. A Light-Up Probe with Aggregation-Induced Emission Characteristics (AIE) for Selective Imaging, Naked-Eye Detection and Photodynamic Killing of Gram-Positive Bacteria. *Chem. Commun.* **2015**, *51*, 12490−12493.
(22) Chen, S.; Li, Q.; Wang, X.; Yang, Y.-W.; Gao, H. Multifunctional Bacterial Imaging and Therapy Systems. *J. Mater. Chem. B* **2018**, *6*, 5198−5214.
(23) Li, Y.; Zhao, Z.; Zhang, J.; Kwok, R. T. K.; Xie, S.; Tang, R.; Jia, Y.; Yang, J.; Wang, L.; Lam, J. W. Y.; Zheng, W.; Jiang, X.; Tang, B. Z. A Bifunctional Aggregation-Induced Emission Luminogen for Monitoring and Killing of Multidrug-Resistant Bacteria. *Adv. Funct. Mater.* **2018**, *28*, 1804632.
(24) Panigrahi, A.; Are, V. N.; Jain, S.; Nayak, D.; Giri, S.; Sarma, T. K. Cationic Organic Nanoaggregates as AIE Luminogens for Wash-Free Imaging of Bacteria and Broad-Spectrum Antimicrobial Application. *ACS Appl. Mater. Interfaces* **2020**, *12*, 5389−5402.
(25) Zhu, Y.; Xu, C.; Wang, Y.; Chen, Y.; Ding, X.; Yu, B. Luminescent Detection of the Lipopolysaccharide Endotoxin and Rapid Discrimination of Bacterial Pathogens Using Cationic Platinum(II) Complexes. *RSC Adv.* **2017**, *7*, 32632−32636.
(26) Mei, J.; Leung, N. L.; Kwok, R. T.; Lam, J. W.; Tang, B. Z. Aggregation-Induced Emission: Together We Shine, United We Soar! *Chem. Rev.* **2015**, *115*, 11718−11940.
(27) Chen, Y.; Lam, J. W. Y.; Kwok, R. T. K.; Liu, B.; Tang, B. Z. Aggregation-Induced Emission: Fundamental Understanding and Future Developments. *Mater. Horiz.* **2019**, *6*, 428−433.
(28) Xu, S.; Duan, Y.; Liu, B. Precise Molecular Design for High-Performance Luminogens With Aggregation-Induced Emission. *Adv. Mater.* **2020**, *32*, 1903530.
(29) Zou, J.; Lu, H.; Zhao, X.; Li, W.; Guan, Y.; Zheng, Y.; Zhang, L.; Gao, H. A Multi-Functional Fluorescent Probe With Aggregation-Induced Emission Characteristics: Mitochondrial Imaging, Photodynamic Therapy and Visualizing Therapeutic Process in Zebrafish Model. *Dyes Pigm.* **2018**, *151*, 45−53.
(30) Mei, J.; Huang, Y.; Tian, H. Progress and Trends in AIE-Based Bioprobes: A Brief Overview. *ACS Appl. Mater. Interfaces* **2018**, *10*, 12217−12261.
(31) Wang, H.; Liu, G. Advances in Luminescent Materials With Aggregation-Induced Emission (AIE) Properties for Biomedical Applications. *J. Mater. Chem. B* **2018**, *6*, 4029−4042.
(32) Gao, M.; Hu, Q.; Feng, G.; Tomczak, N.; Liu, R.; Xing, B.; Tang, B. Z.; Liu, B. A Multifunctional Probe with Aggregation-Induced Emission Characteristics for Selective Fluorescence Imaging and Photodynamic Killing of Bacteria Over Mammalian Cells. *Adv. Healthcare Mater.* **2015**, *4*, 659−663.
(33) Feng, G.; Zhang, C.-J.; Lu, X.; Liu, B. Zinc(II)-Tetradentate-Coordinated Probe With Aggregation-Induced Emission Characteristics for Selective Imaging and Photoinactivation of Bacteria. *ACS Omega* **2017**, *2*, 546−553.
(34) Jain, N.; Alam, P.; Laskar, I. R.; Panwar, J. 'Aggregation Induced Phosphorescence' Active Iridium(III) Complexes for Integrated Sensing and Inhibition of Bacterial Growth in Aqueous Solution. *RSC Adv.* **2015**, *5*, 61983−61988.
(35) Cao, J.-J.; Tan, C.-P.; Chen, M.-H.; Wu, N.; Yao, D.-Y.; Liu, X.-G.; Ji, L.-N.; Mao, Z.-W. Targeting Cancer Cell Metabolism With Mitochondria-Immobilized Phosphorescent Cyclometalated Iridium(III) Complexes. *Chem. Sci.* **2017**, *8*, 631−640.
(36) Zhao, Q.; Huang, C.; Li, F. Phosphorescent Heavy-Metal Complexes for Bioimaging. *Chem. Soc. Rev.* **2011**, *40*, 2508−2524.
(37) Lo, K. K.-W. Luminescent Rhenium(I) and Iridium(III) Polypyridine Complexes as Biological Probes, Imaging Reagents, and Photocytotoxic Agents. *Acc. Chem. Res.* **2015**, *48*, 2985−2995.
(38) Ma, D. L.; Lin, S.; Wang, W.; Yang, C.; Leung, C. H. Luminescent Chemosensors by Using Cyclometalated Iridium(III) Complexes and Their Applications. *Chem. Sci.* **2017**, *8*, 878−889.
(39) Jin, C.; Liu, J.; Chen, Y.; Zeng, L.; Guan, R.; Ouyang, C.; Ji, L.; Chao, H. Cyclometalated Iridium(III) Complexes as Two-Photon Phosphorescent Probes for Specific Mitochondrial Dynamics Tracking in Living Cells. *Chem. - Eur. J.* **2015**, *21*, 12000−12010.
(40) Rietschel, E. T.; Kirikae, T.; Schade, F. U.; Mamat, U.; Schmidt, G.; Loppnow, H.; Ulmer, A. J.; Zahringer, U.; Seydel, U.; Di Padova, F.; Schreier, M.; Brade, H. Bacterial Endotoxin: Molecular Relationships of Structure to Activity and Function. *FASEB J.* **1994**, *8*, 217−225.
(41) Schmidt, R. R.; Pedersen, C. M.; Qiao, Y.; Zähringer, U. Chemical Synthesis of Bacterial Lipoteichoic Acids: an Insight on its Biological Significance. *Org. Biomol. Chem.* **2011**, *9*, 2040−2052.
(42) Yip, A. M.-H.; Lo, K. K.-W. Luminescent Rhenium(I), Ruthenium(II), and Iridium(III) Polypyridine Complexes Containing a Poly(ethylene glycol) Pendant or Bioorthogonal Reaction Group as Biological Probes and Photocytotoxic Agents. *Coord. Chem. Rev.* **2018**, *361*, 138−163.
(43) Chen, F.; Moat, J.; McFeely, D.; Clarkson, G.; Hands-Portman, I. J.; Furner-Pardoe, J. P.; Harrison, F.; Dowson, C. G.; Sadler, P. J. Biguanide Iridium(III) Complexes With Potent Antimicrobial Activity. *J. Med. Chem.* **2018**, *61*, 7330−7344.
(44) Hou, X.-G.; Wu, Y.; Cao, H.-T.; Sun, H.-Z.; Li, H.-B.; Shan, G.-G.; Su, Z.-M. A Cationic Iridium(III) Complex With Aggregation-Induced Emission (AIE) Properties for Highly Selective Detection of Explosives. *Chem. Commun.* **2014**, *50*, 6031−6034.
(45) Xu, P.; Bao, Z.; Yu, C.; Qiu, Q.; Wei, M.; Xi, W.; Qian, Z.; Feng, H. A Water-Soluble Molecular Probe With Aggregation-Induced Emission for Discriminative Detection of $Al^{3+}$ and $Pb^{2+}$ and Imaging in Seedling Root of *Arabidopsis*. *Spectrochim. Acta, Part A* **2019**, *223*, 117335.
(46) Ganesh, V.; Bodewits, K.; Bartholdson, S. J.; Natale, D.; Campopiano, D. J.; Mareque-Rivas, J. C. Effective Binding and Sensing of Lipopolysaccharide: Combining Complementary Pattern Recognition Receptors. *Angew. Chem., Int. Ed.* **2009**, *48*, 356−360.
(47) Wu, J.; Zawistowski, A.; Ehrmann, M.; Yi, T.; Schmuck, C. Peptide Functionalized Polydiacetylene Liposomes Act as a Fluorescent Turn-On Sensor for Bacterial Lipopolysaccharide. *J. Am. Chem. Soc.* **2011**, *133*, 9720−9723.
(48) Zhao, Q.; Li, L.; Li, F.; Yu, M.; Liu, Z.; Yi, T.; Huang, C. Aggregation-Induced Phosphorescent Emission (AIPE) of Iridium(III) Complexes. *Chem. Commun.* **2008**, 685−687.
(49) Galán, L. A.; Cordes, D. B.; Slawin, A. M. Z.; Jacquemin, D.; Ogden, M. I.; Massi, M.; Zysman-Colman, E. Analyzing the Relation between Structure and Aggregation Induced Emission (AIE) Properties of Iridium(III) Complexes through Modification of Non-Chromophoric Ancillary Ligands. *Eur. J. Inorg. Chem.* **2019**, *2019*, 152−163.


https://dx.doi.org/10.1021/acsami.0c11161
ACS Appl. Mater. Interfaces XXXX, XXX, XXX−XXX

(50) Smitten, K. L.; Southam, H. M.; de la Serna, J. B.; Gill, M. R.; Jarman, P. J.; Smythe, C. G. W.; Poole, R. K.; Thomas, J. A. Using Nanoscopy to Probe the Biological Activity of Antimicrobial Leads That Display Potent Activity Against Pathogenic, Multidrug Resistant, Gram-Negative Bacteria. *ACS Nano* **2019**, *13*, 5133−5146.
(51) Zhang, Q.; Cao, R.; Fei, H.; Zhou, M. Mitochondria-Targeting Phosphorescent Iridium(III) Complexes for Living Cell Imaging. *Dalton Trans.* **2014**, *43*, 16872−16879.
(52) Patra, P.; Roy, S.; Sarkar, S.; Mitra, S.; Pradhan, S.; Debnath, N.; Goswami, A. Damage of Lipopolysaccharides in Outer Cell Membrane and Production of ROS-Mediated Stress Within Bacteria Makes Nano Zinc Oxide a Bactericidal Agent. *Appl. Nanosci.* **2015**, *5*, 857−866.
(53) Ong, K. S.; Cheow, Y. L.; Lee, S. M. The Role of Reactive Oxygen Species in the Antimicrobial Activity of Pyochelin. *J. Adv. Res.* **2017**, *8*, 393−398.
(54) Konai, M. M.; Adhikary, U.; Haldar, J. Design and Solution-Phase Synthesis of Membrane-Targeting Lipopeptides With Selective Antibacterial Activity. *Chem. - Eur. J.* **2017**, *23*, 12853−12860.


https://dx.doi.org/10.1021/acsami.0c11161
*ACS Appl. Mater. Interfaces* XXXX, XXX, XXX−XXX